

Reexamining the Relationship between Climate Sensitivity and the Southern Hemisphere Radiation Budget in CMIP Models

KEVIN M. GRISE

Department of Environmental Sciences, University of Virginia, Charlottesville, Virginia

LORENZO M. POLVANI

Department of Applied Physics and Applied Mathematics, Department of Earth and Environmental Sciences, and Lamont-Doherty Earth Observatory, Columbia University, New York, New York

JOHN T. FASULLO

National Center for Atmospheric Research, Boulder, Colorado

(Manuscript received 8 January 2015, in final form 1 September 2015)

ABSTRACT

Recent efforts to narrow the spread in equilibrium climate sensitivity (ECS) across global climate models have focused on identifying observationally based constraints, which are rooted in empirical correlations between ECS and biases in the models' present-day climate. This study reexamines one such constraint identified from CMIP3 models: the linkage between ECS and net top-of-the-atmosphere radiation biases in the Southern Hemisphere (SH).

As previously documented, the intermodel spread in the ECS of CMIP3 models is linked to present-day cloud and net radiation biases over the midlatitude Southern Ocean, where higher cloud fraction in the present-day climate is associated with larger values of ECS. However, in this study, no physical explanation is found to support this relationship. Furthermore, it is shown here that this relationship disappears in CMIP5 models and is unique to a subset of CMIP models characterized by unrealistically bright present-day clouds in the SH subtropics. In view of this evidence, Southern Ocean cloud and net radiation biases appear inappropriate for providing observationally based constraints on ECS.

Instead of the Southern Ocean, this study points to the stratocumulus-to-cumulus transition regions of the SH subtropical oceans as key to explaining the intermodel spread in the ECS of both CMIP3 and CMIP5 models. In these regions, ECS is linked to present-day cloud and net radiation biases with a plausible physical mechanism: models with brighter subtropical clouds in the present-day climate show greater ECS because 1) subtropical clouds dissipate with increasing CO₂ concentrations in many models and 2) the dissipation of brighter clouds contributes to greater solar warming of the surface.

1. Introduction

Equilibrium climate sensitivity (ECS), or the steady-state global-mean surface temperature response to doubled atmospheric CO₂ concentrations, is one of the most widely used metrics for climate change projections. The spread in ECS across the current generation of global climate models [phase 5 of the Coupled Model

Intercomparison Project (CMIP5)] remains large (2.1 to 4.7 K) (Andrews et al. 2012; Forster et al. 2013) and has not notably narrowed from the previous generation of models (CMIP3; Randall et al. 2007), or even from the early pioneering estimates of Charney (1979). Recently, many studies have focused on identifying observationally based constraints to help narrow the spread in ECS across models (e.g., Knutti et al. 2006; Trenberth and Fasullo 2010; Huber et al. 2011; Fasullo and Trenberth 2012; Sherwood et al. 2014; Tian 2015). These studies identify physically motivated empirical correlations between ECS and biases in the present-day climate of models, estimate realistic values of these biased climate

Corresponding author address: Kevin M. Grise, Department of Environmental Sciences, University of Virginia, 291 McCormick Road, P.O. Box 400123, Charlottesville, VA 22904-4123.
E-mail: kmg3r@virginia.edu

properties using observations, and then provide more limited bounds on ECS using these observational constraints. Importantly, such constraints on ECS must be supported by sound physical hypotheses, as large correlations between present-day climate properties and ECS might occur by chance in models (Caldwell et al. 2014).

Most of these studies have emphasized the role of model biases in the tropics and subtropics in contributing to the intermodel spread in ECS. For example, Fasullo and Trenberth (2012) found a significant correlation in CMIP3 models between ECS and the present-day subtropical-to-tropical relative humidity contrast during the boreal summer monsoon season, with only the models with the highest values of ECS having the most realistic relative humidity contrast between the tropics and subtropics (i.e., strong enough subtropical dry zones). Recently, Sherwood et al. (2014) pointed to the strength of low to midlevel convective mixing in the tropical and subtropical troposphere, with only the CMIP3 and CMIP5 models with higher values of ECS having values of convective mixing in the present-day climate consistent with observational estimates.

In this paper, we revisit one study that instead emphasized the role of the Southern Hemisphere (SH) midlatitudes in contributing to the intermodel spread in ECS. Trenberth and Fasullo (2010, hereafter TF10) demonstrated that most CMIP3 models overestimate the absorbed solar radiation over the Southern Ocean, leading to a surplus of net downward top-of-the-atmosphere radiation in the SH. As a result, models that simulated a strong increase in cloud amount in this region with global warming were hypothesized to be implausible given the already high cloud fraction (>80%) observed. To support their hypothesis, TF10 found a strong anticorrelation in CMIP3 models between present-day biases in SH net radiation and ECS, with the models having the largest biases in net radiation having the smallest values of ECS (cf. Fig. 13 of TF10; see also Fig. 1a). Hence, the models with the largest values of ECS (greater than 4 K) were deemed to be the most realistic. However, TF10 remained unsure whether this relationship between the SH radiation biases and ECS was causal, or merely an artifact of the models they examined. Additionally, subsequent studies have showed that reductions in absorbed solar radiation over the Southern Ocean in global warming simulations are primarily due to increases in cloud albedo rather than increases in cloud fraction (Soden and Vecchi 2011; Zelinka et al. 2012, 2013; Kay et al. 2014).

Here, we show that the relationship identified by TF10 in CMIP3 models largely disappears in CMIP5 models. We demonstrate that the correlation between

ECS and SH radiation biases in CMIP3 models arises not only from the Southern Ocean but also from the SH subtropics. Furthermore, we illustrate that the correlation occurs only in models with large subtropical cloud biases, which include almost all CMIP3 models but only a fraction of CMIP5 models. Consequently, we suggest that the relationship noted by TF10 does not derive from a robust physical relationship in the climate system, but instead could be symptomatic of the unrealistic representation of certain key physical processes in a subset of current climate models.

The paper is organized as follows. Section 2 details the data and methods used in this study. Section 3 compares and contrasts the relationships among ECS, net top-of-the-atmosphere radiation biases, and cloud-radiative properties in CMIP3 and CMIP5 models. Section 4 then clarifies the key findings by partitioning the models into categories based on their subtropical cloud biases. Section 5 provides a discussion of the results, and section 6 concludes with a summary.

2. Data and methods

The primary data used in this study are the monthly-mean output from the global climate models that participated in CMIP3 (Meehl et al. 2007) and CMIP5 (Taylor et al. 2012), provided courtesy of the Program for Climate Model Diagnosis and Intercomparison (PCMDI) at Lawrence Livermore National Laboratory. We use output from 14 CMIP3 models and 20 CMIP5 models (see Table 1 for list of models). The models are selected using the same three criteria as Grise and Polvani (2014). First, the model's ECS is defined in Randall et al. (2007) (for 19 CMIP3 models) or Forster et al. (2013) (for 23 CMIP5 models). Second, three different forcing scenarios (as listed below) are available for all variables used in this study.¹ Third, the model must exhibit a local minimum in shortwave cloud-radiative effect at SH midlatitudes (as in the observed climatology).² For each of the models, we analyze three different forcing scenarios: 1) preindustrial control (i.e., hundreds of years of unforced variability), 2) twentieth-century simulations (20C3M for CMIP3, historical for

¹ For CMIP3 models, CGCM3.1(T63) does not have 1% yr⁻¹ scenario integrations available, ECHO-G does not have zonal wind available from either its control or twentieth-century integrations, and MRI-CGCM2.3.2 does not have total cloud fraction available from its control integration. For CMIP5 models, FGOALS-s2 does not have historical scenario integrations available.

² For CMIP5 models, GISS-E2-H and GISS-E2-R are excluded (see Grise and Polvani 2014).

TABLE 1. Listing of CMIP3 and CMIP5 models used in this study. The second column lists values of ECS from [Randall et al. \(2007\)](#) for CMIP3 models and [Forster et al. \(2013\)](#) for CMIP5 models. The third column lists the present-day (1990–99 mean) subtropical shortwave cloud-radiative effect (CRE) averaged over the green-boxed regions in [Fig. 4b](#) (as plotted in [Fig. 4c](#)). Expansions of acronyms are available online at <http://www.ametsoc.org/PubsAcronymList>.

Model name	ECS (K)	Present-day subtropical shortwave CRE (W m^{-2})
CMIP3 models		
CCSM3	2.7	−50.90
CGCM3.1 (T47)	3.4	−54.33
CSIRO Mk3.0	3.1	−60.86
ECHAM5/MPI	3.4	−46.76
GFDL-CM2.0	2.9	−60.35
GFDL-CM2.1	3.4	−55.02
GISS-EH	2.7	−53.64
INM-CM3.0	2.1	−47.65
IPSL-CM4	4.4	−43.36
MIROC3.2 (hires)	4.3	−62.35
MIROC3.2 (medres)	4.0	−62.17
NCAR PCM1	2.1	−56.49
UKMO-HadCM3	3.3	−52.61
UKMO-HadGEM1	4.4	−44.11
CMIP5 models		
ACCESS1.0	3.83	−43.55
BCC-CSM1.1	2.82	−48.02
BCC-CSM1.1-m	2.87	−54.06
CanESM2	3.69	−47.78
CCSM4	2.89	−41.10
CNRM-CM5	3.25	−42.34
CSIRO-Mk3.6.0	4.08	−58.90
GFDL-CM3	3.97	−46.46
GFDL-ESM2G	2.39	−51.66
GFDL-ESM2M	2.44	−52.83
HadGEM2-ES	4.59	−43.13
INM-CM4	2.08	−36.94
IPSL-CM5A-LR	4.13	−50.91
IPSL-CM5B-LR	2.61	−42.90
MIROC5	2.72	−66.23
MIROC-ESM	4.67	−62.80
MPI-ESM-LR	3.63	−44.51
MPI-ESM-P	3.45	−44.10
MRI-CGCM3	2.60	−44.44
NorESM1-M	2.80	−49.41

CMIP5), and 3) integrations with $1\% \text{ yr}^{-1}$ increases in atmospheric CO_2 concentrations until CO_2 is doubled from preindustrial levels. We have additionally excluded two CMIP3 models (FGOALS-g1.0 and GISS-ER), which appear to have incorrectly applied the $1\% \text{ yr}^{-1}$ CO_2 increase scenario and do not show appreciable global-mean surface temperature warming over the duration of the run. For all scenarios, we use the first ensemble member (“run1” from CMIP3, “r1i1p1” from CMIP5) from each model.

To compare the model output with observations, we make use of two observational datasets: 1) monthly-mean top-of-the-atmosphere radiative fluxes from the Clouds and Earth’s Radiant Energy System (CERES) experiment [Energy Balance and Filled (EBAF) top-of-the-atmosphere fluxes version 2.8; [Loeb et al. 2012](#)] obtained from the NASA Langley Research Center, and 2) monthly-mean visible-infrared satellite-detected cloud fractions from the International Satellite Cloud Climatology Project (ISCCP; [Rossow and Schiffer 1999](#)) obtained from the NASA Goddard Institute for Space Studies. Following [TF10](#), we define the present-day climatology of the models using the 1990–99 period from the twentieth-century simulations, and the present-day climatology of the observations using the March 2000–October 2005 period from the CERES and ISCCP datasets.

We calculate three variables using the CERES and model radiative fluxes. First, net downward top-of-the-atmosphere radiation (R_{net}) is defined as the absorbed solar radiation minus the outgoing longwave radiation at the top of the atmosphere. Second, the shortwave cloud-radiative effect (CRE) is defined as the difference in outgoing shortwave radiation at the top of the atmosphere between clear-sky and all-sky scenes (e.g., [Ramanathan et al. 1989](#)). Third, cloud albedo (α_{cloud}) is defined using the formula

$$\alpha_{\text{cloud}} = \frac{\alpha - (1-f)\alpha_{\text{clear}}}{f}, \quad (1)$$

where α is the top-of-the-atmosphere all-sky albedo, α_{clear} is the top-of-the-atmosphere clear-sky albedo, and f is the total cloud fraction.

Statistical significance of the results is assessed using a Student’s t test, which implicitly assumes that each model is independent from the other models. In reality, the degrees of freedom are much fewer, as individual models share components with other models of the same generation and with models of previous generations ([Masson and Knutti 2011](#); [Knutti et al. 2013](#)). However, assessing statistical significance in this manner is still useful, as results that fail to be significant assuming model independence would also fail to be significant with many fewer degrees of freedom.

3. Relationships among climate sensitivity, net radiation biases, and cloud-radiative properties in CMIP models

In this section, we examine in detail the relationship between ECS and the present-day climatology of SH net downward top-of-the-atmosphere radiation (R_{net}) in both CMIP3 and CMIP5 models. To begin, in [Fig. 1a](#), we reproduce the results from [Fig. 13](#) of [TF10](#), plotting the

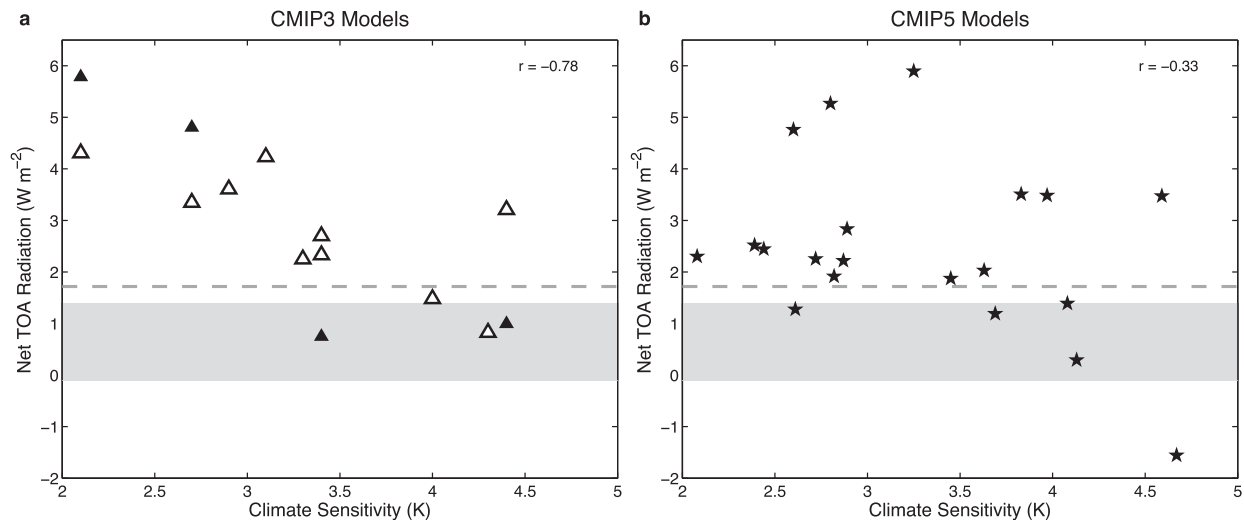


FIG. 1. Scatterplot between (abscissa) equilibrium climate sensitivity (ECS) and (ordinate) 1990–99 mean net top-of-the-atmosphere (TOA) radiation (R_{net}) (averaged over the Southern Hemisphere) for (a) CMIP3 models (denoted by triangles) and (b) CMIP5 models (denoted by stars). The unfilled symbols denote the models used in TF10. The gray shaded region denotes the observational bounds on SH R_{net} used by TF10, and the gray dashed line denotes the climatological estimate (March 2000–October 2005) on SH R_{net} from the most recent version of the CERES dataset (version 2.8).

ECS of CMIP3 models versus R_{net} averaged over the entire SH in the present-day (1990–99 mean) climate. As discussed in TF10, there is a significant anticorrelation between ECS and SH R_{net} , both in the subset of models used by TF10 (unfilled triangles in Fig. 1a) and in all 14 CMIP3 models examined here ($r = -0.78$). And, as identified by TF10, only those models with the highest values of ECS possess values of SH R_{net} consistent with those observed in the present-day climate.

Figure 1b shows an analogous scatterplot to Fig. 1a, but for CMIP5 models. In contrast to CMIP3 models, the correlation between ECS and SH R_{net} in CMIP5 models is much weaker ($r = -0.33$) and is no longer statistically significant at the 95% confidence level. In fact, the correlation largely depends on the behavior of one model (MIROC-ESM) with a very large negative value of SH R_{net} ; the correlation drops to $r = -0.12$ when this model is excluded. And, unlike the CMIP3 models, CMIP5 models with both low and high values of ECS possess values of SH R_{net} similar to those observed in the present-day climate.

So, why does the relationship in Fig. 1 weaken substantially in CMIP5 models? We seek further insight by exploring the geographic distribution of the correlations between ECS and R_{net} in Fig. 2a. In CMIP3 models, two main geographic regions contribute to the large negative correlation seen in Fig. 1a. First, as emphasized by TF10, there are large anticorrelations between ECS and present-day R_{net} over the Southern Ocean (Fig. 2, black boxed region). But, equally large anticorrelations also

occur in the stratocumulus-to-cumulus transition regions of the SH subtropical ocean basins (Fig. 2, green boxed regions). Note that these subtropical regions are similar to those emphasized by Fasullo and Trenberth (2012) and Sherwood et al. (2014). In CMIP5 models, the anticorrelations remain comparable in the SH subtropical regions but are much weaker and no longer statistically significant over the Southern Ocean (Fig. 2a, right). Additionally, significant positive correlations between ECS and present-day R_{net} biases are present over the Maritime Continent, South America, and southern Africa in CMIP5 models, which are not present in CMIP3 models.

The regions of significant anticorrelations between ECS and SH R_{net} in Fig. 2a primarily occur over cloud-covered oceans. To confirm the role of clouds in the correlations, in Fig. 2b we show the correlations of ECS with the present-day climatology of shortwave CRE for CMIP3 and CMIP5 models. The correlations of ECS with shortwave CRE largely mirror those with R_{net} (Fig. 2a), with significant anticorrelations over both the Southern Ocean and SH subtropical oceans in CMIP3 models but only over the subtropical oceans in CMIP5 models. The bulk of the correlations over the Southern Ocean arise from variations in total cloud fraction across the models (Fig. 2c); that is, models with larger cloud fraction over the Southern Ocean generally have higher climate sensitivity. In contrast, the bulk of the correlations over the SH subtropical oceans arise from variations in cloud albedo (Fig. 2d); that is, models with

1990–1999 Climatology: Correlations with Equilibrium Climate Sensitivity

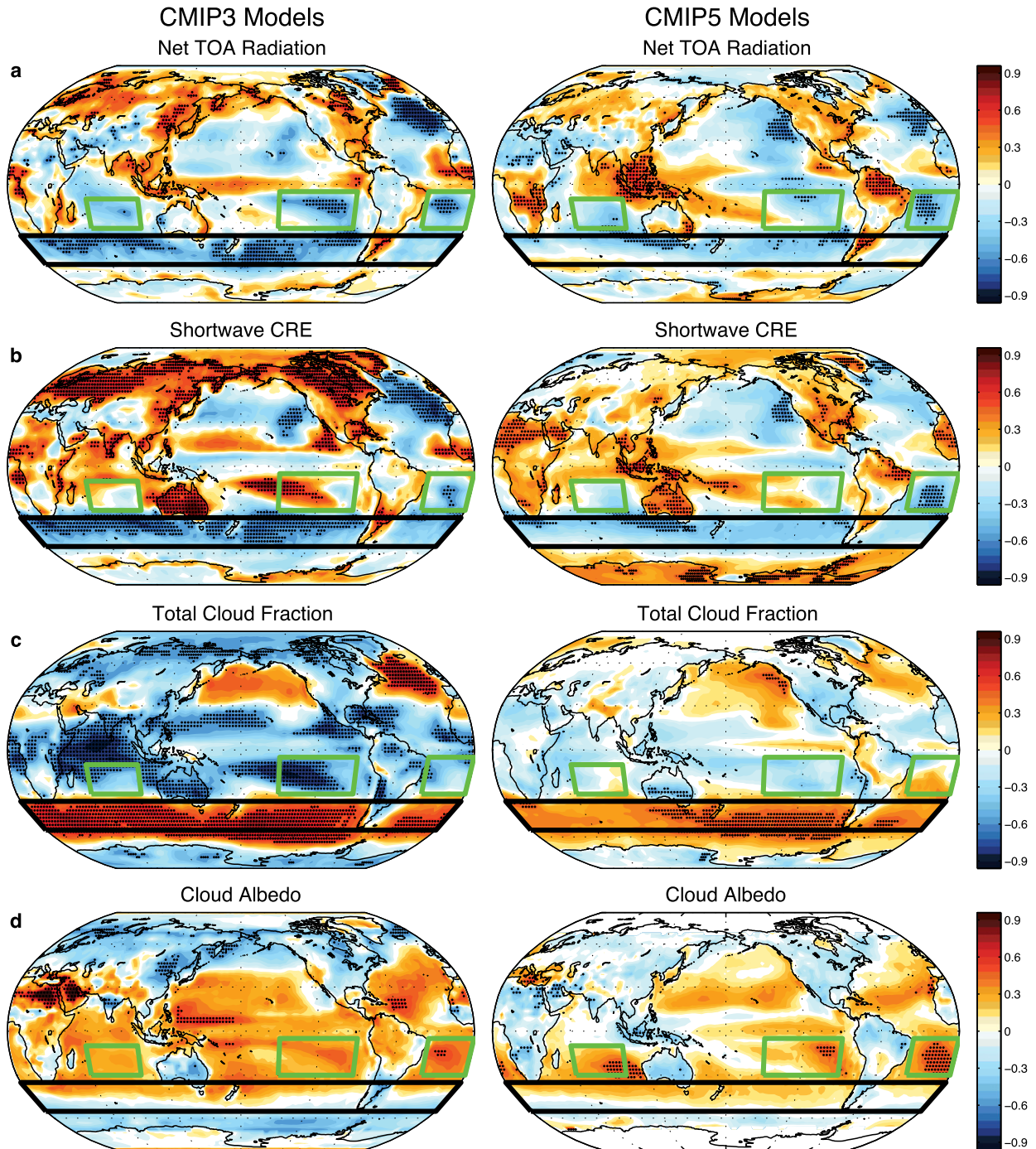


FIG. 2. Correlations between ECS and the 1990–99 mean value of (a) R_{net} , (b) shortwave cloud–radiative effect (CRE), (c) total cloud fraction, and (d) cloud albedo at each grid point, for (left) CMIP3 and (right) CMIP5 models. The contour interval is 0.06. The stippling indicates regions where the correlation coefficient is 95% significant using Student's t test. The green (black) boxes isolate SH subtropical (Southern Ocean) regions examined in subsequent figures.

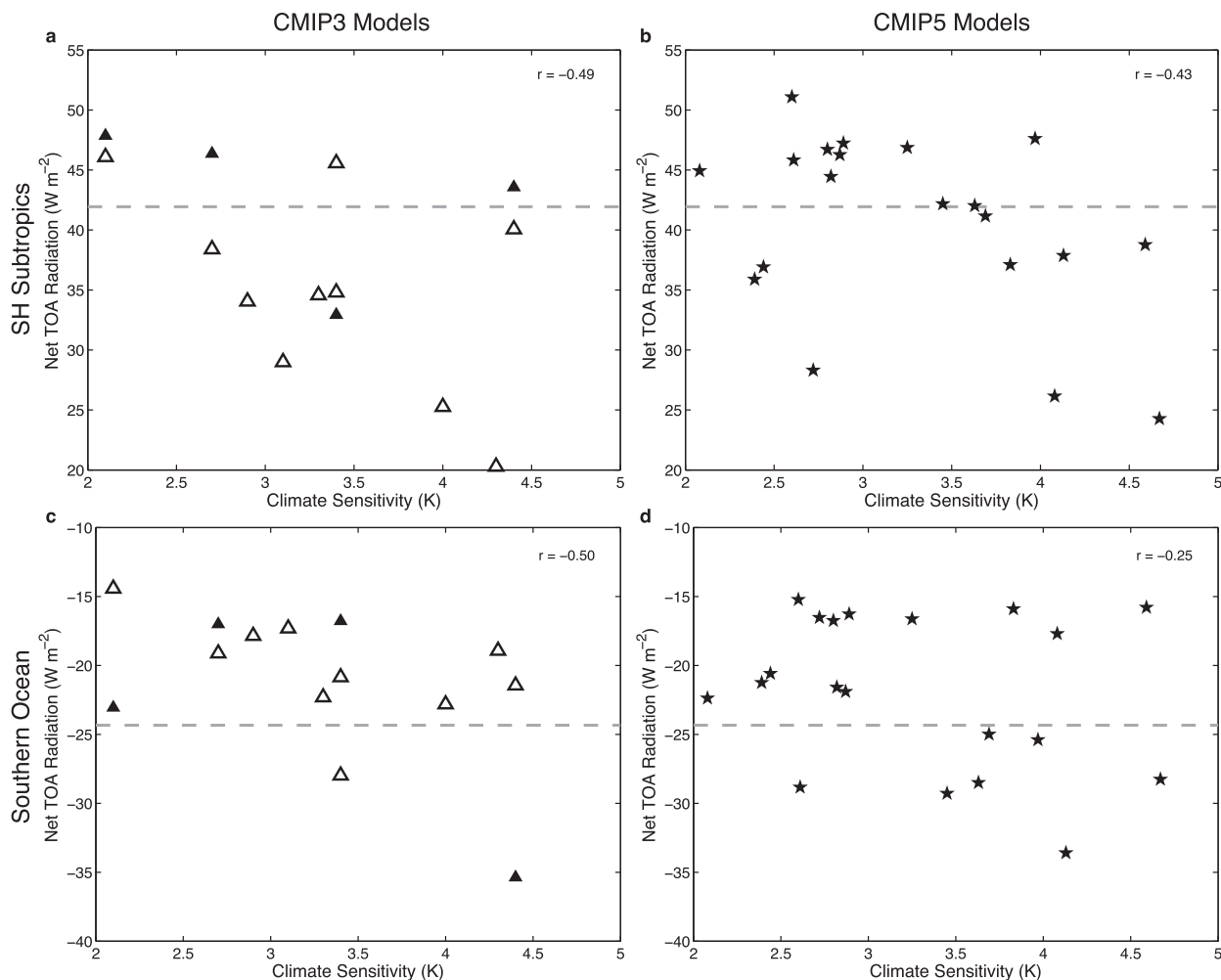


FIG. 3. As in Fig. 1, but for scatterplots between ECS and R_{net} averaged over (top) the SH subtropical regions indicated by green boxes in Fig. 2 and (bottom) the Southern Ocean region (35° – 55° S) indicated by the black box in Fig. 2.

brighter clouds over the SH subtropical oceans generally have higher climate sensitivity. We note that correlations of present-day total (longwave + shortwave) CRE with ECS are very similar to those shown in Figs. 2a and 2b, indicating the dominant role of low-level clouds in the correlation patterns. One exception is over the subtropical South Pacific in CMIP3 models, where the longwave (high cloud) effect appears to dominate.

To summarize the relative contributions of the SH subtropics and Southern Ocean, in Fig. 3 we reproduce the scatterplots between ECS and present-day R_{net} shown in Fig. 1, but now average R_{net} only over the two specific regions identified from Fig. 2: the SH subtropical ocean basins (Fig. 2, green boxed regions) and the Southern Ocean (Fig. 2, black boxed region). Consistent with Fig. 2, there are sizable negative correlations ($r \approx -0.50$) between ECS and R_{net} in both regions in

CMIP3 models, but only in the subtropical regions in CMIP5 models. When compared to the latest CERES satellite climatology (Fig. 3, dashed lines), the CMIP3 models on average overestimate R_{net} over the Southern Ocean and underestimate R_{net} in the SH subtropical regions (TF10; see also Table 2). Consequently, in CMIP3 models, the sign of the correlations is such that the higher ECS models have more realistic values of R_{net} over the Southern Ocean (as emphasized by TF10; Fig. 3c), but the *lower* ECS models have more realistic values of R_{net} over the SH subtropics (Fig. 3a). Hence, the hemispheric-mean relationship in Fig. 1a is somewhat misleading, as it results from the cancellation of influences from the subtropics and Southern Ocean. Furthermore, we note that there is little evidence from CMIP5 models to suggest that either high or low ECS models have more realistic present-day values of SH R_{net} (Figs. 1b and 3b,d).

TABLE 2. Present-day climatological values of net downward top-of-the-atmosphere radiation (R_{net}), shortwave CRE, total cloud fraction, and cloud albedo averaged over the Southern Ocean (35° – 55° S; black boxed region in Fig. 2) and SH subtropics (green boxed regions in Fig. 2). The present-day values are derived from the 1990–99 mean climate for the models, and the March 2000–October 2005 mean climate for the observations (following TF10). For the models, the multimodel mean value is given ± 1 standard deviation.

	Observations	CMIP3 models	CMIP5 models
Southern Ocean			
R_{net} (W m^{-2})	–24.34	-21.09 ± 5.35	-21.87 ± 5.61
Shortwave CRE (W m^{-2})	–68.26	-68.36 ± 8.23	-66.48 ± 9.69
Total cloud fraction (%)	83.82	68.51 ± 6.69	68.43 ± 7.54
Cloud albedo	0.40	0.47 ± 0.03	0.47 ± 0.03
SH subtropics			
R_{net} (W m^{-2})	41.94	37.05 ± 8.47	40.58 ± 7.48
Shortwave CRE (W m^{-2})	–41.55	-53.61 ± 6.47	-48.60 ± 7.47
Total cloud fraction (%)	56.65	51.99 ± 9.34	50.61 ± 6.82
Cloud albedo	0.28	0.37 ± 0.06	0.35 ± 0.05

The results in Figs. 2 and 3 suggest that the breakdown of the relationship in Fig. 1 in CMIP5 models may be tied, at least in part, to the Southern Ocean. Although the correlations between ECS and present-day R_{net} biases in the SH subtropics are comparable in CMIP3 and CMIP5 models (Figs. 2a and 3a,b), the correlations between ECS and present-day R_{net} biases over the Southern Ocean are much weaker in CMIP5 models than in CMIP3 models (Figs. 2a and 3d). Consequently, one might expect that Southern Ocean R_{net} and cloud biases have been notably reduced from CMIP3 to CMIP5 models. Surprisingly, however, neither the multimodel mean nor the intermodel variance of Southern Ocean R_{net} , shortwave CRE, cloud fraction, or cloud albedo has substantially improved in CMIP5 models (see Table 2). The CMIP5 models continue to have an extremely large intermodel spread in shortwave CRE over the Southern Ocean, to underestimate total cloud fraction, and to overestimate R_{net} and cloud

albedo (e.g., Ceppi et al. 2012; Wang and Su 2013; Klein et al. 2013). In fact, the intermodel variance in Southern Ocean R_{net} , shortwave CRE, and total cloud fraction is actually larger in the CMIP5 models examined here (Table 2).

Instead, the results in Table 2 reveal that CMIP5 models had more systematic improvement in the SH subtropical regions (Fig. 2, green boxed regions). Figure 4 shows the multimodel mean difference in the present-day climatologies of R_{net} and shortwave CRE between CMIP3 and CMIP5 models. One can easily see significant increases in R_{net} and shortwave CRE in the stratocumulus-to-cumulus transition regions of the SH subtropical ocean basins in CMIP5 models (Fig. 4, green boxed regions), exactly the same subtropical regions where the anticorrelations between R_{net} and ECS are large (Fig. 2a, green boxed regions). The significant increases in R_{net} and shortwave CRE in these regions in CMIP5 models arise from a reduction in both total cloud fraction and cloud albedo (Table 2; see also Klein et al. 2013).

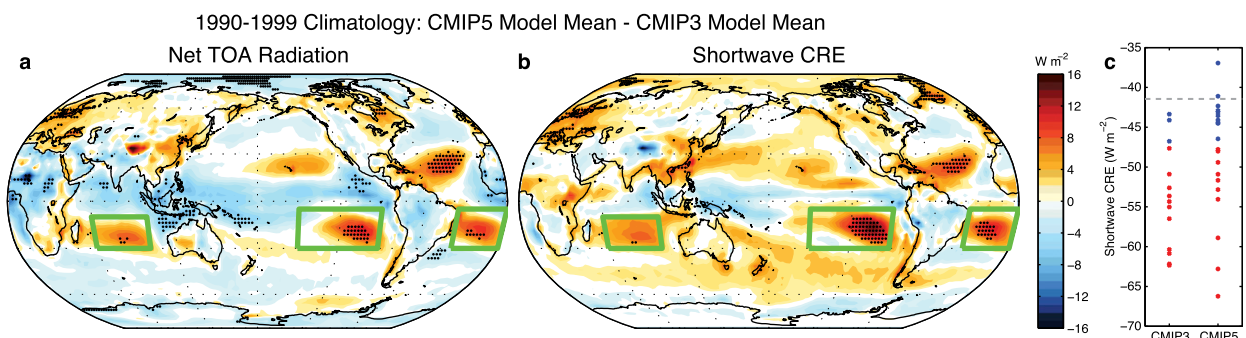


FIG. 4. Difference in the 1990–99 mean values of (a) R_{net} and (b) shortwave CRE between CMIP3 and CMIP5 models. The contour interval is 1 W m^{-2} , and the stippling indicates regions where the difference is 95% significant using a Student's t test. (c) The values of shortwave CRE averaged over the green-boxed subtropical regions in (b). Models with values less (greater) than the median value of CMIP5 models are plotted in red (blue). The gray dashed line denotes the CERES climatological-mean value for the period March 2000–October 2005.

To summarize, TF10 noted a strong relationship between ECS and present-day SH-mean R_{net} biases in CMIP3 models (Fig. 1a). We have shown here that 1) this hemispheric-mean relationship arises from the competing influences of two geographic regions, the SH subtropics and Southern Ocean (Figs. 2a and 3), and that 2) it largely disappears in CMIP5 models (Fig. 1b). At first glance, the weakening of the hemispheric-mean relationship in CMIP5 models does not appear tied to the SH subtropical regions, where correlations between ECS and present-day cloud and radiation biases are comparable in CMIP3 and CMIP5 models (Figs. 2 and 3a,b). Instead, the weakening of the hemispheric-mean relationship appears tied, at least in part, to the Southern Ocean, where correlations between ECS and present-day cloud and radiation biases are much weaker in CMIP5 models than in CMIP3 models (Figs. 2 and 3c,d). But, perplexingly, Southern Ocean cloud and radiation biases have not notably improved from CMIP3 to CMIP5 models, and SH subtropical cloud and radiation biases have significantly improved from CMIP3 to CMIP5 models (Fig. 4; Table 2). In the next section, we resolve these seemingly contradictory results and demonstrate that the subtropical improvements in CMIP5 models are in fact linked to the breakdown of the TF10 relationship in CMIP5 models.

4. Partitioning CMIP models by subtropical cloud-radiative effect bias

In this section, we investigate whether the significant reductions in subtropical R_{net} and cloud biases from CMIP3 to CMIP5 models (Fig. 4) are linked to the weakening of the correlation between ECS and present-day SH-mean R_{net} biases in CMIP5 models (Fig. 1). To test this, we divide the CMIP5 models into two subsets: one subset of 10 models with a present-day mean shortwave CRE in the SH subtropical regions that is less than the CMIP5 median value (Fig. 4c, red circles) and another subset of 10 models with a present-day mean shortwave CRE in the SH subtropical regions that is greater than the CMIP5 median value (Fig. 4c, blue circles). The first subset of models possesses large negative biases in the present-day values of SH subtropical shortwave CRE (as in the CMIP3 models), and for short we refer to these models hereafter as the “more subtropically biased” models. The second subset of models possesses present-day values of SH subtropical shortwave CRE more similar to observations (Fig. 4c, gray dashed line), and we refer to these models hereafter as the “less subtropically biased” models. For reference, the values of present-day mean shortwave CRE in the SH subtropical regions for all models are listed in the

third column of Table 1. Note that all but three CMIP3 models have a present-day mean value that is less than the CMIP5 median value, and thus most CMIP3 models fall into the more subtropically biased category (Fig. 4c; Table 1).

Figure 5 shows the correlations between ECS and the models’ present-day cloud and radiation climatologies (as in Fig. 2), but now for the two subsets of CMIP5 models. For the more subtropically biased CMIP5 models (Fig. 5a, left), there are significant anticorrelations between ECS and the present-day values of R_{net} over both the Southern Ocean and SH subtropical regions, as in CMIP3 models (cf. Figs. 5a and 2a). However, for the less subtropically biased CMIP5 models (Fig. 5a, right), the significant anticorrelations are confined to the subtropics. Similarly, the present-day values of shortwave CRE over the Southern Ocean are significantly anticorrelated with ECS in only the more subtropically biased CMIP5 models (cf. Figs. 5b and 2b), and the present-day values of total cloud fraction over the Southern Ocean are significantly correlated with ECS in only the more subtropically biased CMIP5 models (cf. Figs. 5c and 2c). Both subsets of CMIP5 models possess large correlations between ECS and present-day cloud albedo in the subtropics (Fig. 5d). Hence, the behavior of the subset of CMIP5 models with larger subtropical biases (i.e., more negative values of subtropical shortwave CRE; Fig. 5, left) is strongly reminiscent of that of CMIP3 models (Fig. 2, left).

As further evidence of this, in Fig. 6 we reproduce the scatterplots between ECS and present-day R_{net} from Figs. 1 and 3, but with the more subtropically biased models plotted in red and the less subtropically biased models plotted in blue. Consistent with the results in Fig. 5, a strong, significant negative correlation exists between ECS and present-day SH R_{net} in the more subtropically biased CMIP3 and CMIP5 models ($r = -0.80$; Fig. 6a, red), with only the highest ECS models having present-day values of SH R_{net} comparable to observations (as noted by TF10 for CMIP3 models). In contrast, the less subtropically biased models show little correlation between ECS and SH R_{net} ($r = -0.03$; Fig. 6a, blue). Likewise, from Fig. 6c we see that the correlation between ECS and present-day R_{net} over the Southern Ocean is only found in the more subtropically biased models (see also Fig. 5a, left).

From Fig. 6b, we see that the correlation between ECS and present-day R_{net} in the SH subtropics is present in both subsets of models (see also Fig. 5a, green boxes), suggesting that the linkage between bright subtropical clouds in the present-day climate and higher values of ECS is robust across multiple generations of CMIP models (Figs. 2d and 5d). Interestingly, the slope of this

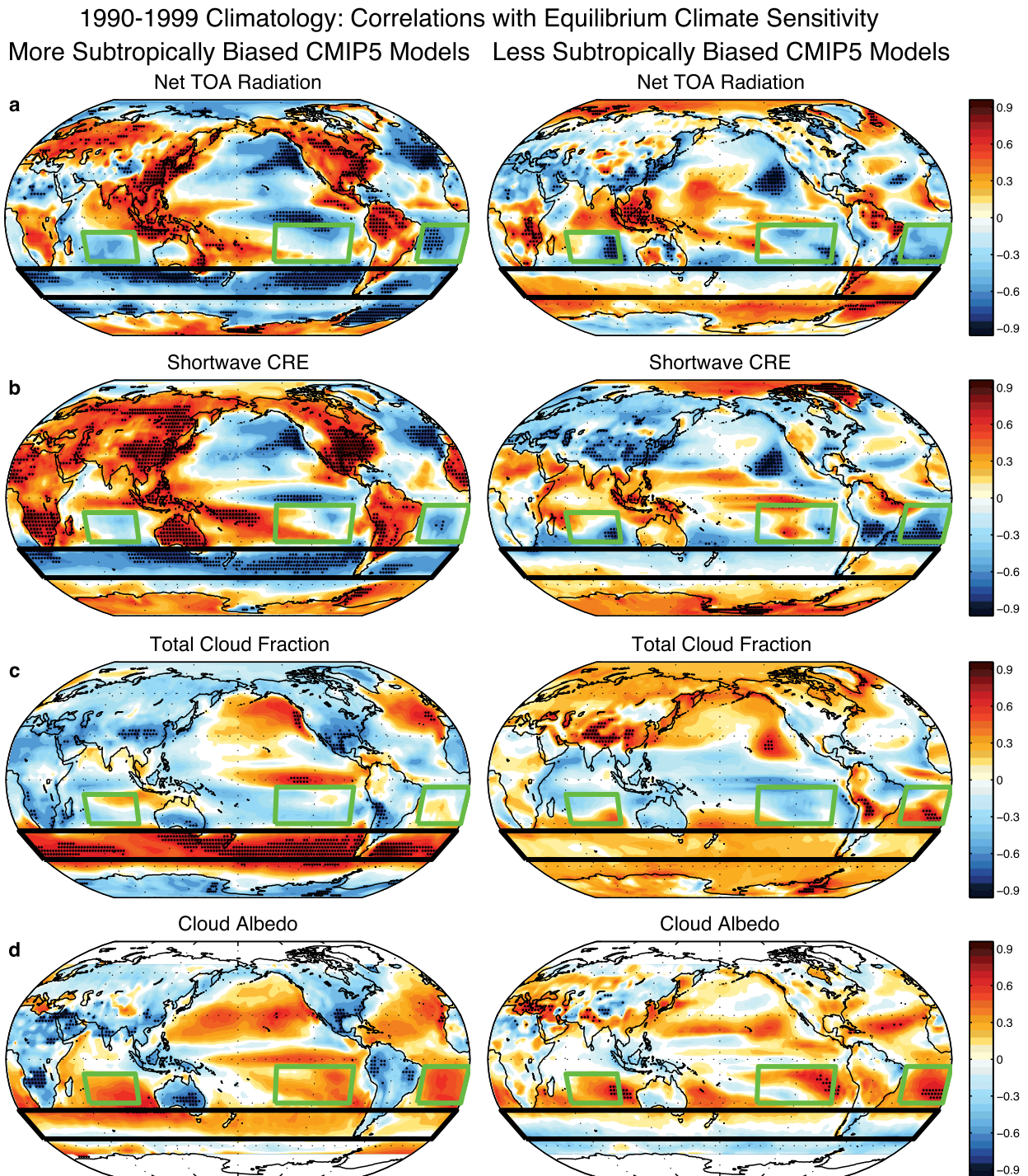


FIG. 5. As in Fig. 2, but for (left) the CMIP5 models with more negative present-day values of subtropical shortwave CRE (red circles in Fig. 4c) and (right) the CMIP5 models with less negative present-day values of subtropical shortwave CRE (blue circles in Fig. 4c).

relationship is very different in the two subsets of models. In the more subtropically biased models (Fig. 6b, red), the *lower* ECS models have more realistic present-day values of R_{net} in the SH subtropics (as noted

above for CMIP3 models), but in the less subtropically biased models (Fig. 6b, blue) the *higher* ECS models have more realistic present-day values of R_{net} in the SH subtropics.

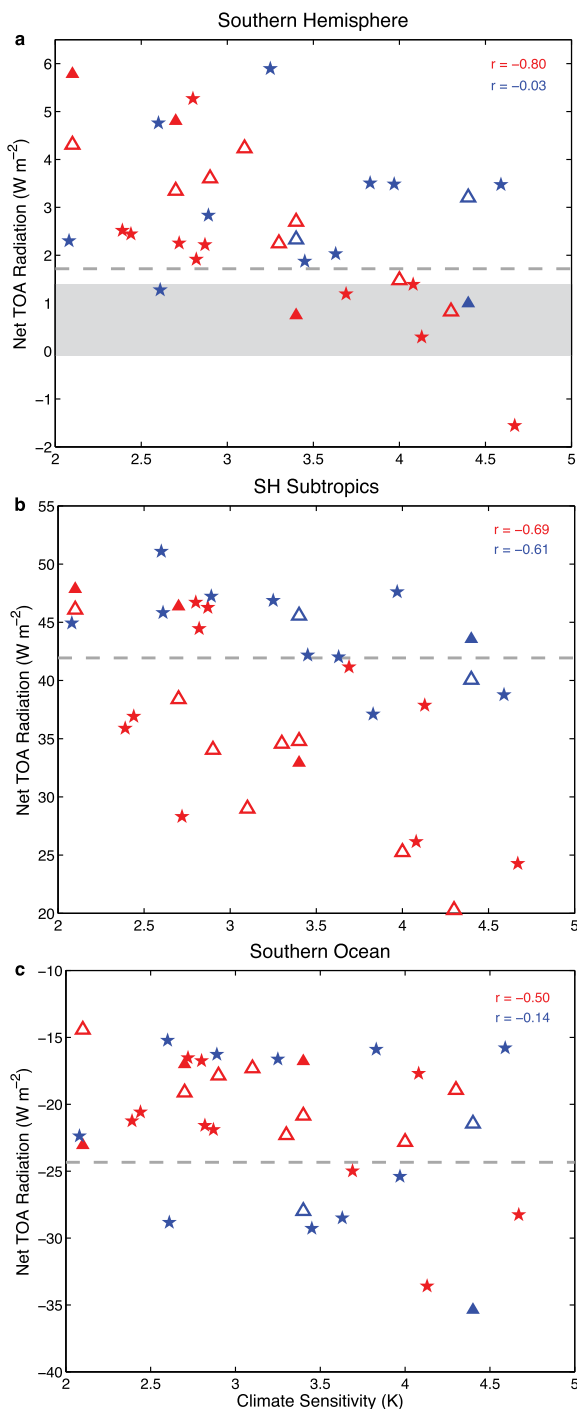


FIG. 6. (a) As in Fig. 1, (b) as in the top row of Fig. 3, and (c) as in the bottom row of Fig. 3, but colored according to the present-day values of subtropical shortwave CRE (see Fig. 4c). Models with more (less) negative present-day values of subtropical shortwave CRE are in red (blue). Triangles denote CMIP3 models, and stars denote CMIP5 models.

In summary, the results in this section have demonstrated that the relationship between ECS and present-day SH R_{net} biases noted by TF10 is unique to a particular subset of models, which 1) includes nearly all CMIP3 models and a good fraction of CMIP5 models (Fig. 6a, red) and 2) is characterized by strongly negatively biased shortwave CRE in the stratocumulus-to-cumulus transition regions of the SH subtropics (Fig. 4c, red). Irrespective of the subtropical cloud biases, CMIP models with brighter present-day subtropical clouds (and thus more negative values of subtropical R_{net}) are associated with larger values of ECS (Figs. 5a,d and 6b). But, it is only in CMIP models with large present-day *subtropical* shortwave CRE biases that Southern Ocean (and consequently SH mean) R_{net} biases are correlated with ECS (Figs. 5a and 6a,c). In the following section, we explore the physical mechanisms underlying these relationships.

5. Discussion

The results in the previous sections have been purely diagnostic. First, we have shown that ECS is linked to present-day SH R_{net} biases in CMIP3 models in two regions: the Southern Ocean and the stratocumulus-to-cumulus transition regions of the SH subtropics (Figs. 2a and 3). Second, we have shown that the subtropical component of this relationship is robust across CMIP3 and CMIP5 models, as models with brighter clouds in the present-day climate are associated with larger values of ECS (Figs. 2d and 6b). And third, we have shown that the Southern Ocean component of this relationship only appears in models with large subtropical cloud biases (Fig. 5, left; Fig. 6c, red). However, we have not yet addressed whether these correlations are physically meaningful, or whether they are merely artifacts of the models.

To better understand why the present-day model biases discussed above are linked with ECS, in Fig. 7 we examine the correlations of ECS with the responses of shortwave CRE and total cloud fraction to doubled atmospheric CO_2 concentrations. Here, the response to doubled atmospheric CO_2 concentrations is defined as the difference between the preindustrial control climatology of each model and the year 51–70 mean of the corresponding $1\% \text{ yr}^{-1}$ CO_2 increase run (i.e., the average of the 20 years leading up to CO_2 doubling). To be clear, this response to doubled atmospheric CO_2 concentrations encompasses both the direct radiative response to CO_2 forcing as well as the response to the accompanying sea surface temperature increases. One limitation to using the $1\% \text{ yr}^{-1}$ CO_2 increase runs is that they are transient runs, meaning that the ocean has not

2xCO₂ Response: Correlations with Equilibrium Climate Sensitivity CMIP3 Models

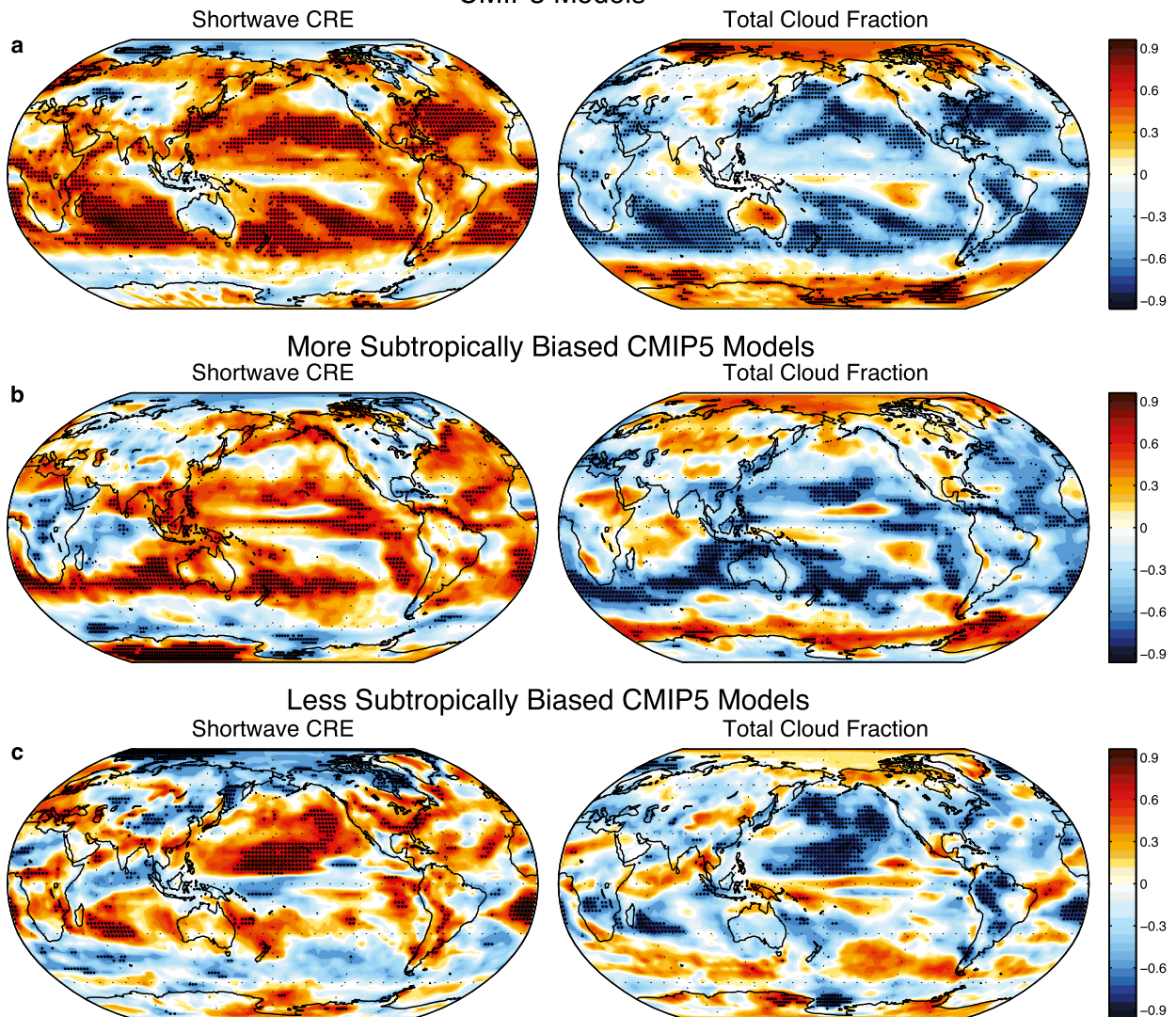


FIG. 7. Correlations between ECS and the response of (left) shortwave CRE and (right) total cloud fraction to doubled atmospheric CO₂ concentrations, for (a) CMIP3 models, (b) the CMIP5 models with more negative present-day values of subtropical shortwave CRE (red circles in Fig. 4c), and (c) the CMIP5 models with less negative present-day values of subtropical shortwave CRE (blue circles in Fig. 4c). The contour interval is 0.06. The stippling indicates regions where the correlation coefficient is 95% significant using Student's *t* test.

fully adjusted to the applied CO₂ forcing. Nonetheless, these runs are the only climate change experiments available in both the CMIP3 and CMIP5 ensembles that can be directly compared, as they use identical forcings to assess the climate's response to increased atmospheric CO₂ concentrations.

In response to doubled atmospheric CO₂ concentrations, CMIP models exhibit highly variable shortwave cloud feedbacks over tropical and subtropical oceans (e.g., Bony and Dufresne 2005; Vial et al. 2013). In CMIP3 models and the more subtropically biased

CMIP5 models, increases in shortwave CRE throughout the SH subtropics are significantly correlated with ECS (Figs. 7a,b, left). As noted by Soden and Vecchi (2011), models with the highest values of ECS strongly reduce low-level marine clouds in most regions of the subtropics as CO₂ increases, whereas models with the lowest values of ECS actually increase low-level marine clouds in some subtropical regions (see Fig. 7, right). For the less subtropically biased CMIP5 models, the correlations between ECS and the changes in shortwave CRE and total cloud fraction are not as large, significant, or

spatially extensive as in the more subtropically biased models (cf. Fig. 7c with Figs. 7a and 7b). For both CMIP3 and CMIP5 models, changes in cloud albedo have a much weaker relationship with ECS than the changes in cloud fraction (not shown; see also Soden and Vecchi 2011).

The results in Fig. 7 make clear that the dissipation of low-level clouds throughout large regions of the subtropics under enhanced CO₂ conditions is closely tied to high ECS in both CMIP3 and CMIP5 models (Fig. 7, right; Webb et al. 2006; Soden and Vecchi 2011; Vial et al. 2013). The dissipation of highly reflective subtropical clouds should have a larger positive impact on shortwave CRE than the dissipation of less reflective subtropical clouds (e.g., compare the left panels of Figs. 7b and 7c). Thus, it seems logical that models with brighter present-day clouds in the subtropics (and hence smaller values of present-day R_{net}) could contribute to greater global-mean surface temperature warming than models with dimmer subtropical clouds (Figs. 2d and 5d). Consequently, we suggest that the correlations between ECS and present-day R_{net} biases in the SH subtropics are physically meaningful because 1) they survive across multiple generations of CMIP models (Figs. 3a,b and 6b) and 2) they can be explained by a plausible physical mechanism.

In contrast, the results in Fig. 7 show little evidence that the response of Southern Ocean clouds to enhanced CO₂ conditions is strongly correlated with ECS, in either CMIP3 or CMIP5 models. This is somewhat surprising given that, in the more subtropically biased models, there is a large correlation between ECS and Southern Ocean cloud fraction in the present-day climatology (Figs. 2c and 5c), which contributes to the sizeable anti-correlation between ECS and present-day R_{net} there (Figs. 2a and 5a). Consequently, we suggest that the correlations between ECS and present-day R_{net} biases over the Southern Ocean originally emphasized in TF10 are merely accidental because 1) they do not survive across multiple generations of CMIP models and 2) they lack a clear physical linkage with the response of Southern Ocean clouds to enhanced CO₂ conditions. Our results confirm the speculation by TF10 that the relationship in Fig. 1a is “merely symptomatic of other things going on in the model and is not the explanation of either the sensitivity or the errors in the SH.” From this, we conclude that negative biases in Southern Ocean cloud amount are not first-order indicators of ECS.

We close by addressing one remaining question: Why are models with large present-day subtropical cloud biases associated with correlations between ECS and present-day biases over the Southern Ocean? The answer to this question likely lies in the fact that cloud

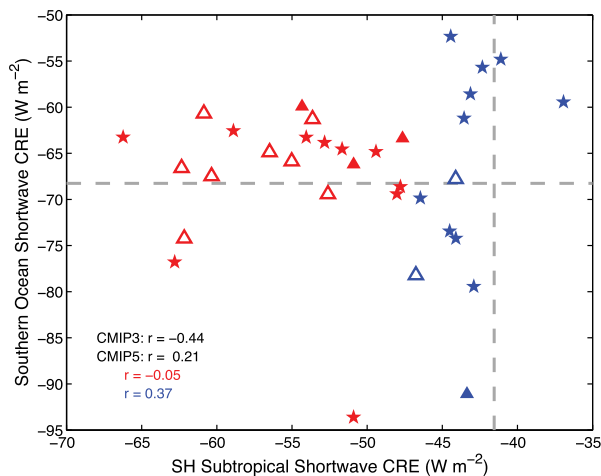


FIG. 8. Scatterplot between the 1990–99 mean value of (abscissa) shortwave CRE averaged over the SH subtropical regions indicated by the green boxes in Fig. 2 and (ordinate) shortwave CRE averaged over the Southern Ocean region (35°–55°S) indicated by the black box in Fig. 2. The symbols are the same as in Fig. 6. The gray dashed lines denote the observational climatological estimates from CERES.

properties in the low cloud regimes of the SH subtropics and midlatitudes are not independent of one another in CMIP models. Figure 8 shows the scatterplot of the present-day values of shortwave CRE averaged over the SH subtropics (Fig. 2, green boxed regions) and Southern Ocean (Fig. 2, black boxed region) for both CMIP3 and CMIP5 models. In the more subtropically biased models (Fig. 8, red), the scatter generally falls along a horizontal line. In these models, the values of Southern Ocean shortwave CRE cluster relatively close to the CERES observational estimate (Fig. 8, gray horizontal line), whereas the values of subtropical shortwave CRE are widely spread across the models. In contrast, in the less subtropically biased models (Fig. 8, blue), the scatter generally falls along a vertical line. In these models, the values of subtropical shortwave CRE cluster relatively close to the CERES observational estimate (Fig. 8, gray vertical line), whereas the values of Southern Ocean shortwave CRE are now much more poorly constrained.

The trade-off between a better representation of present-day Southern Ocean or subtropical shortwave CRE in these subsets of models points to choices made in the model development process, rather than robust physical processes. For example, in the more subtropically biased models (Fig. 8, red), it appears as if the present-day values of Southern Ocean shortwave CRE have been tuned to the observations, as models with larger present-day cloud albedo over the Southern Ocean generally have lower cloud fraction there

($r = -0.53$). In the less subtropically biased models (Fig. 8, blue), the present-day values of Southern Ocean shortwave CRE deviate greatly from observations, and there is no longer compensation between present-day values of total cloud fraction and cloud albedo in individual models ($r = 0.31$).

Interestingly, in the more subtropically biased models, the present-day value of Southern Ocean cloud albedo is also correlated with the present-day values of cloud albedo ($r = 0.46$) and total cloud fraction ($r = -0.79$) in the SH *subtropical* regions. In the less subtropically biased models, these correlations are much weaker ($r = 0.29$ and $r = -0.25$, respectively). We have no way of verifying whether correlations between subtropical and midlatitude cloud properties occur in the observed climate system on long time scales, but we find no evidence that these relationships exist in observed month-to-month variability. Using nearly a decade (March 2000–December 2009) of CERES and ISCCP monthly-mean anomalies (i.e., anomalies about the mean seasonal cycle), we find that variability in observed Southern Ocean cloud albedo is only weakly correlated with variability in SH subtropical cloud albedo ($r = 0.07$) and SH subtropical cloud fraction ($r = -0.18$). Consequently, we find no clear physical reason to expect a linkage between subtropical cloud biases and the correlations between ECS and present-day biases over the Southern Ocean. Instead, the linkage between subtropical and midlatitude cloud properties is likely an artifact of choices made in model parameterization and tuning, as illustrated in Fig. 8.

6. Summary and conclusions

In this paper, we have reexamined the relationship between equilibrium climate sensitivity (ECS) and net top-of-the-atmosphere radiation (R_{net}) biases in the Southern Hemisphere in CMIP models, as first identified by TF10. They showed that, among CMIP3 models, only those models with the highest values of ECS possess realistic present-day values of SH-mean R_{net} (Fig. 1a), which they attributed to excess absorbed solar radiation over the Southern Ocean in lower ECS models. Here, we have shown that although Southern Ocean cloud and radiation biases have not been reduced from CMIP3 to CMIP5 models, the relationship noted by TF10 largely disappears in CMIP5 models (Fig. 1b). Furthermore, we have demonstrated that this relationship is intimately tied not only to the Southern Ocean, but also—and most importantly—to the stratocumulus-to-cumulus transition regions of the SH subtropics (Fig. 2a), where cloud and radiation biases have notably improved in CMIP5 models.

Our findings lead us to conclude that the Southern Ocean component of the TF10 relationship arises as an artifact of a particular class of climate models with excessively reflective present-day subtropical clouds, which includes most CMIP3 models but only a fraction of CMIP5 models (Fig. 6c, red). For this subset of models, models with larger present-day Southern Ocean cloud fraction are associated with larger values of ECS (Figs. 2c and 5c). However, these correlations do not survive in CMIP5 models with less subtropically biased clouds (Fig. 5, right), and no physical mechanism has been found linking present-day Southern Ocean biases with global-mean surface temperature warming under enhanced CO_2 conditions (Fig. 7a). In view of these results, we conclude that present-day Southern Ocean cloud and radiation biases should not be viewed as fundamental indicators of the intermodel spread in ECS.

Instead, in agreement with many previous studies, we find that the subtropics have a more important role in the intermodel spread in ECS (e.g., Bony and Dufresne 2005; Soden and Vecchi 2011; Fasullo and Trenberth 2012; Vial et al. 2013; Sherwood et al. 2014). The subtropical component of the TF10 relationship is more robust, as it survives across multiple generations of CMIP models and is supported by a plausible physical mechanism. For both CMIP3 and CMIP5 models, models with brighter present-day subtropical clouds are associated with larger values of ECS (Fig. 2d). Under enhanced CO_2 conditions, cloud fraction decreases throughout the subtropics in many models, so the models with the brightest clouds in the present-day climate exhibit the greatest global-mean surface temperature response (Fig. 7a). However, while the relationship between ECS and present-day subtropical radiation biases is robust in both CMIP3 and CMIP5 models, its intercept with observations is not: CMIP5 models with the most realistic present-day values of SH subtropical R_{net} have larger values of ECS than their CMIP3 counterparts (cf. Figs. 3a and 3b). Thus, we are not advocating that this relationship is appropriate for providing observational constraints on ECS.

Identifying large model biases in fields physically linked to climate feedbacks remains a promising path for improving models and for potentially narrowing their spread in ECS. In particular, using present-day climatological biases in fields that set the local environment for cloud formation might be particularly effective (Fasullo and Trenberth 2012; Sherwood et al. 2014), as the cloud fields themselves are often tuned (as illustrated here in Fig. 8). However, as model physics continue to improve, it is likely that the causes of ECS spread among model ensembles will also evolve. Consequently, one might not necessarily expect empirical

correlations between ECS and present-day climate properties identified for one generation of models (such as the one identified by TF10 for CMIP3) to be the same as those identified for the next generation. Klocke et al. (2011) reached a similar conclusion when comparing results from a single-model perturbed parameter ensemble with the CMIP3 multimodel ensemble. Correlations that survive across multiple generations of models, and that are supported by testable physical mechanisms, are the only ones that should be used to constrain ECS (see also Sherwood et al. 2014). Nonetheless, caution is clearly needed when linking any empirical relationship to observations: when the correlation between ECS and a present-day climate property arises from a systematic model bias rather than from a real physical process, its utility becomes questionable.

Acknowledgments. We thank M. Zelinka and two anonymous reviewers for helpful comments on the manuscript. We acknowledge WCRP's Working Group on Coupled Modelling, which is responsible for CMIP, and we thank the climate modeling groups (listed in Table 1) for producing and making available their model output. For CMIP, the U.S. Department of Energy's PCMDI provides coordinating support and led development of software infrastructure in partnership with the Global Organization for Earth System Science Portals. L.M.P. is supported by a National Science Foundation grant to Columbia University.

REFERENCES

- Andrews, T., J. M. Gregory, M. J. Webb, and K. E. Taylor, 2012: Forcing, feedbacks, and climate sensitivity in CMIP5 coupled atmosphere–ocean climate models. *Geophys. Res. Lett.*, **39**, L09712, doi:10.1029/2012GL051607.
- Bony, S., and J.-L. Dufresne, 2005: Marine boundary layer clouds at the heart of tropical cloud feedback uncertainties in climate models. *Geophys. Res. Lett.*, **32**, L20806, doi:10.1029/2005GL023851.
- Caldwell, P. M., C. S. Bretherton, M. D. Zelinka, S. A. Klein, B. D. Santer, and B. M. Sanderson, 2014: Statistical significance of climate sensitivity predictors obtained by data mining. *Geophys. Res. Lett.*, **41**, 1803–1808, doi:10.1002/2014GL059205.
- Ceppi, P., Y.-T. Hwang, D. M. W. Frierson, and D. L. Hartmann, 2012: Southern Hemisphere jet latitude biases in CMIP5 models linked to shortwave cloud forcing. *Geophys. Res. Lett.*, **39**, L19708, doi:10.1029/2012GL053115.
- Charney, J. G., 1979: *Carbon Dioxide and Climate: A Scientific Assessment*. National Academies Press, 34 pp.
- Fasullo, J., and K. Trenberth, 2012: A less cloudy future: The role of subtropical subsidence in climate sensitivity. *Science*, **338**, 792–794, doi:10.1126/science.1227465.
- Forster, P. M., T. Andrews, P. Good, J. M. Gregory, L. S. Jackson, and M. Zelinka, 2013: Evaluating adjusted forcing and model spread for historical and future scenarios in the CMIP5 generation of climate models. *J. Geophys. Res. Atmos.*, **118**, 1139–1150, doi:10.1002/jgrd.50174.
- Grise, K. M., and L. M. Polvani, 2014: Southern Hemisphere cloud-dynamics biases in CMIP5 models and their implications for climate projections. *J. Climate*, **27**, 6074–6092, doi:10.1175/JCLI-D-14-00113.1.
- Huber, M., I. Mahlstein, M. Wild, J. Fasullo, and R. Knutti, 2011: Constraints on climate sensitivity from radiation patterns in climate models. *J. Climate*, **24**, 1034–1052, doi:10.1175/2010JCLI3403.1.
- Kay, J. E., B. Medeiros, Y.-T. Hwang, A. Gettelman, J. Perket, and M. G. Flanner, 2014: Processes controlling Southern Ocean shortwave climate feedbacks in CESM. *Geophys. Res. Lett.*, **41**, 616–622, doi:10.1002/2013GL058315.
- Klein, S. A., Y. Zhang, M. D. Zelinka, R. Pincus, J. Boyle, and P. J. Gleckler, 2013: Are climate model simulations of clouds improving? An evaluation using the ISCCP simulator. *J. Geophys. Res. Atmos.*, **118**, 1329–1342, doi:10.1002/jgrd.50141.
- Klocke, D., R. Pincus, and J. Quaas, 2011: On constraining estimates of climate sensitivity with present-day observations through model weighting. *J. Climate*, **24**, 6092–6099, doi:10.1175/2011JCLI4193.1.
- Knutti, R., G. A. Meehl, M. R. Allen, and D. A. Stainforth, 2006: Constraining climate sensitivity from the seasonal cycle in surface temperature. *J. Climate*, **19**, 4224–4233, doi:10.1175/JCLI3865.1.
- , D. Masson, and A. Gettelman, 2013: Climate model genealogy: Generation CMIP5 and how we got there. *Geophys. Res. Lett.*, **40**, 1194–1199, doi:10.1002/grl.50256.
- Loeb, N. G., S. Kato, W. Su, T. Wong, F. G. Rose, D. R. Doelling, J. R. Norris, and X. Huang, 2012: Advances in understanding top-of-atmosphere radiation variability from satellite observations. *Surv. Geophys.*, **33**, 359–385, doi:10.1007/s10712-012-9175-1.
- Masson, D., and R. Knutti, 2011: Climate model genealogy. *Geophys. Res. Lett.*, **38**, L08703, doi:10.1029/2011GL046864.
- Meehl, G. A., C. Covey, T. Delworth, M. Latif, B. McAvaney, J. F. B. Mitchell, R. J. Stouffer, and K. E. Taylor, 2007: The WCRP CMIP3 multimodel dataset: A new era in climate change research. *Bull. Amer. Meteor. Soc.*, **88**, 1383–1394, doi:10.1175/BAMS-88-9-1383.
- Ramanathan, V., R. D. Cess, E. F. Harrison, P. Minnis, B. R. Barkstrom, E. Ahmad, and D. Hartmann, 1989: Cloud-radiative forcing and climate: Results from the Earth Radiation Budget Experiment. *Science*, **243**, 57–63, doi:10.1126/science.243.4887.57.
- Randall, D. A., and Coauthors, 2007: Climate models and their evaluation. *Climate Change 2007: The Physical Science Basis*, S. Solomon et al., Eds., Cambridge University Press, 591–662.
- Rossow, W. B., and R. A. Schiffer, 1999: Advances in understanding clouds from ISCCP. *Bull. Amer. Meteor. Soc.*, **80**, 2261–2287, doi:10.1175/1520-0477(1999)080<2261:AIUCFI>2.0.CO;2.
- Sherwood, S. C., S. Bony, and J.-L. Dufresne, 2014: Spread in model climate sensitivity traced to atmospheric convective mixing. *Nature*, **505**, 37–42, doi:10.1038/nature12829.
- Soden, B. J., and G. A. Vecchi, 2011: The vertical distribution of cloud feedback in coupled ocean–atmosphere models. *Geophys. Res. Lett.*, **38**, L12704, doi:10.1029/2011GL047632.
- Taylor, K. E., R. J. Stouffer, and G. A. Meehl, 2012: An overview of CMIP5 and the experiment design. *Bull. Amer. Meteor. Soc.*, **93**, 485–498, doi:10.1175/BAMS-D-11-00094.1.

- Tian, B., 2015: Spread of model climate sensitivity linked to double-intertropical convergence zone bias. *Geophys. Res. Lett.*, **42**, 4133–4141, doi:[10.1002/2015GL064119](https://doi.org/10.1002/2015GL064119).
- Trenberth, K. E., and J. T. Fasullo, 2010: Simulation of present-day and twenty-first-century energy budgets of the Southern Oceans. *J. Climate*, **23**, 440–454, doi:[10.1175/2009JCLI3152.1](https://doi.org/10.1175/2009JCLI3152.1).
- Vial, J., J.-L. Dufresne, and S. Bony, 2013: On the interpretation of inter-model spread in CMIP5 climate sensitivity estimates. *Climate Dyn.*, **41**, 3339–3362, doi:[10.1007/s00382-013-1725-9](https://doi.org/10.1007/s00382-013-1725-9).
- Wang, H., and W. Su, 2013: Evaluating and understanding top of the atmosphere cloud radiative effects in Intergovernmental Panel on Climate Change (IPCC) Fifth Assessment Report (AR5) Coupled Model Intercomparison Project phase 5 (CMIP5) models using satellite observations. *J. Geophys. Res. Atmos.*, **118**, 683–699, doi:[10.1029/2012JD018619](https://doi.org/10.1029/2012JD018619).
- Webb, M. J., and Coauthors, 2006: On the contribution of local feedback mechanisms to the range of climate sensitivity in two GCM ensembles. *Climate Dyn.*, **27**, 17–38, doi:[10.1007/s00382-006-0111-2](https://doi.org/10.1007/s00382-006-0111-2).
- Zelinka, M. D., S. A. Klein, and D. L. Hartmann, 2012: Computing and partitioning cloud feedbacks using cloud property histograms. Part II: Attribution to changes in cloud amount, altitude, and optical depth. *J. Climate*, **25**, 3736–3754, doi:[10.1175/JCLI-D-11-00249.1](https://doi.org/10.1175/JCLI-D-11-00249.1).
- , —, K. E. Taylor, T. Andrews, M. J. Webb, J. M. Gregory, and P. M. Forster, 2013: Contributions of different cloud types to feedbacks and rapid adjustments in CMIP5. *J. Climate*, **26**, 5007–5027, doi:[10.1175/JCLI-D-12-00555.1](https://doi.org/10.1175/JCLI-D-12-00555.1).